Supporting Information

Heterogeneous crystalline-amorphous interface for boosted electrocatalytic nitrogen reduction to ammonia

Yuchi Wan,‡[a] Zhijie Wang,‡[b] Muyun Zheng,[a] Jia Li*[bd] and Ruitao Lv*[ac]

[a] State Key Laboratory of New Ceramics and Fine Processing, School of Materials Science and Engineering, Tsinghua University, Beijing, 100084, China

[b] Shenzhen Geim Graphene Center and Institute of Materials Research, Tsinghua Shenzhen International Graduate School, Tsinghua University, Shenzhen 518055, China

[c] Key Laboratory of Advanced Materials (MOE), School of Materials Science and Engineering, Tsinghua University, Beijing, 100084, China

[d] Guangdong Provincial Key Laboratory of Thermal Management Engineering and Materials, Tsinghua Shenzhen International Graduate School, Tsinghua University, Shenzhen 518055, China

* Corresponding authors.

E-mail address: lvruitao@tsinghua.edu.cn (Ruitao Lv), li.jia@sz.tsinghua.edu.cn (Jia Li).

‡ Yuchi Wan and Zhijie Wang contributed equally to this work.

Experimental Procedures

Chemicals: Bismuth chloride (Macklin, $BiCl_3$, AR), ammonium heptamolybdate tetrahydrate (Aladdin, $(NH_4)_6Mo_7O_{24} \cdot 4H_2O$, 99.9%), sodium borohydride (Aladdin, $NaBH_4$, 98%), sodium sulfate (Sinopharm Chemical Reagent Co., Ltd, Na_2SO_4, AR), ethanol absolute (Sinopharm Chemical Reagent Co., Ltd, C_2H_6O, AR), acetone (Beijing Chemical Works, C_3H_6O, AR), isopropanol (Sinopharm Chemical Reagent Co., Ltd, C_3H_8O, AR), ammonium chloride (Sinopharm Chemical Reagent Co., Ltd, NH_4Cl, AR), sodium hypochlorite aqueous solution (Sinopharm Chemical Reagent Co., Ltd, $NaClO$, CP), sodium hydroxide (Beijing Chemical Works, $NaOH$, AR), sodium citrate (Sinopharm Chemical Reagent Co., Ltd, $C_6H_5Na_3O_7$, 98%), salicylic acid (Sinopharm Chemical Reagent Co., Ltd, $C_7H_6O_3$, AR), sodium nitroprusside dihydrate (Sinopharm Chemical Reagent Co., Ltd, $Na_2[Fe(CN)_5NO] \cdot 2H_2O$, AR), hydrazine hydrate (Sinopharm Chemical Reagent Co., Ltd, $N_2H_4 \cdot H_2O$, 85%), sulfuric acid (Beijing Chemical Works, H_2SO_4, AR), hydrochloric acid (Beijing Chemical Works, HCl, AR), p-Dimethylaminobenzaldehyde (Energy Chemical, $C_9H_{11}NO$, 98%). Ultrapure water used throughout all experiments was purified through a Millipore system. Ultra-high purity N_2 (99.999%) and Ar (99.999%) were purchased from PRAXAIR.

Sample characterizations: X-ray diffraction (XRD) patterns were collected by a Rigaku D/max-2500 using Cu Kα radiation (λ=1.5406 Å, 40 kV, and 150 mA). Scanning electron microscopy (SEM) images were obtained by a field emission scanning electron microscope (GeminiSEM 500), which was equipped with an energy dispersive spectroscopy (EDS,

Extreme) detector. Information on the microstructures and fringes was obtained via transmission electron microscope (TEM) (JEOL JEM-2100F) with a field emission gun operating at 200 kV, and elemental-mapping information was obtained by the corresponding EDS. X-ray photoelectron spectroscopy (XPS) was collected by scanning X-ray microprobe (ESCALAB 250Xi, Thermo Fisher Scientific.) to analyze the chemical states of the elements, and the binding energies of all elements were calibrated by using the C1s peak of adventitious carbon at 284.80 eV. Raman data were collected on a HORIBA LabRAM HR Evolution spectroscopy using the excitation wavelength of 532 nm. Nitrogen adsorption-desorption tests were carried out on the Belshop-mini II surface and the porosity analyzer, and specific surface areas were calculated through the Brunaure-Emmert-Teller (BET) method. Pore volumes and sizes were calculated from the pore-size distribution curves by the density functional theory (DFT) law. The absorbance data of the spectrophotometer were collected on the SHIMADZU UV-2450 ultraviolet-visible (UV-vis) spectrophotometer. Temperature-programmed desorption of N_2 (N_2-TPD) experiment was conducted on a Quantachrome Chem BET Pulsar TPR/TPD. 20 mg catalyst was first pretreated at 150 °C for 1 h in pure He with a flow rate of 50 mL/min and then cooled down to room temperature in He. The catalyst adsorbed N_2 for 1 h, and the remaining N_2 was purged by He for half an hour with a flow rate of 50 mL/min. Finally, the desorption of N_2 was carried out by heating from room temperature to 800 °C at a rate of 10 °C/min to record the N_2-TPD profile. X-ray absorption spectroscopy (XAS) analysis was performed with Si (111) crystal monochromators at the BL14W1 beamlines at the

Shanghai Synchrotron Radiation Facility (SSRF) (Shanghai, China). The XAS spectra were recorded at room temperature using a 4-channel Silicon Drift Detector (SDD) Bruker 5040. Negligible changes in the line-shape and peak position of Bi L_3-edge XANES spectra were observed between two scans taken for a specific sample. The XAS spectra of these standard samples (Bi foil and Bi_2O_3) were recorded in transmission mode. The spectra were processed and analyzed by the software codes Athena and Artemis.

Working electrode preparation and electrochemical tests in H-cell: Prior to the working electrode preparation, the $1.0×1.5$ cm^2 carbon cloth (CeTech Taiwan, NOS10025) was washed with acetone, ethanol, and deionized water to clean the surface impurities, followed by the surface treatment in air plasma environment to increase the hydrophilia of carbon cloth. For the working electrode preparation, 1 mg catalyst was dispersed in the mixture of 470 μL isopropanol and 30 μL Nafion solution (5wt%). The mixture was sonicated for 1 h to form a uniform catalyst ink. 50 μL of the resulting catalyst ink was drop-casted onto a carbon cloth with a loading area of $1×1$ cm^2, and the final mass loading was calculated to be 0.1 mg cm^{-2}.

All electrochemical N_2 reduction reaction (NRR) experiments were carried out with an electrochemical workstation (Bio-Logic Science EC-LAB) at room temperature. An H-type cell was used in this work, in which two chambers are separated by a Nafion 115 membrane. In order to eliminate possible ammonia contamination, the Nafion 115 membrane was pretreated by sonicating in 0.05 M H_2SO_4 for 10 minutes before any electrochemical tests. The electrochemical experiments were carried out *via* a three-electrode configuration (the working

electrode of the carbon cloth loading catalysts, the counter electrode of Pt foil, and the reference electrode of Ag/AgCl (3.5 M KCl)). 30 mL 0.10 M Na_2SO_4 was used as electrolytes, which were purged with ultra-high purity N_2 (99.999%) for 30 min before N_2 reduction measurement, and then bubbled with a constant flow rate of 20 mL min^{-1} throughout the whole electrolysis process. Due to the high solubility of ammonia in aqueous solution, the downstream acid trap was not implemented in this work. All potentials were referenced against the reversible hydrogen electrode (RHE) based on the Nernst equation ($E_{RH} = E_{Ag/AgCl\ (3.5\ M\ KCl)} + 0.059 \times pH + 0.205$). Linear sweep voltammogram (LSV) measurements were performed from -0.2 V to -0.6 V vs. RHE at a scan rate of 5 mV s^{-1}. For NRR experiments, potentiostatic tests were conducted at different potentials ranging from -0.2 V to -0.6 V vs. RHE for 2h. After the entire reduction reaction was terminated, the electrolyte was collected to detect the ammonia product.

Ammonia quantification: The concentration of synthesized ammonia via the electrocatalytic NRR was determined by the indophenol blue method. In the indophenol blue method, 2 mL electrolyte was removed from the electrochemical reaction vessel after the electrolysis process and added into 2 mL NaOH solution (1 M) containing 5 % salicylic acid and 5 % sodium citrate (by weight), and then followed by addition of 1 mL NaClO (0.05 M) and 0.2 mL $C_5FeN_6Na_2O$ aqueous solution (1wt%). After standing in darkness for 2 hours, the absorption spectrum was measured using a UV-vis spectrophotometer. The formation of indophenol blue was determined using absorbance at a wavelength of 655 nm. The concentration-absorbance curves were calibrated using standard solutions: 0.1 M Na_2SO_4 electrolyte with a series of

concentrations of NH₄Cl. The standard curve was plotted with the absorbance values at a wavelength of 655 nm on the *y-axis* and the concentration of NH_3 on the *x-axis*. The obtained standard curve ($y = 0.013 + 0.342x$, $R^2=0.999$) shows a good linear relation of absorbance value with NH_3 concentration.

^{15}N isotopic labeling measurement: The $^{15}N_2$ isotopic labeling experiment was carried out using $^{15}N_2$ as the feeding gas (WUHAN NEWRADAR SPECIAL GAS Co., LTD., 99 atom% ^{15}N) with 0.1 M Na_2SO_4 electrolyte. Before electrolysis, ultra-high purity Ar (99.999%) was purged for 30 min to remove $^{14}N_2$. Then $^{15}N_2$ was pre-purified by flowing through 0.05 M H_2SO_4 solution to remove N contamination, and purged for 30 min to saturate the electrolyte. After $^{15}N_2$ electroreduction for 2 h at -0.4 V *vs*. RHE in 0.1 M Na_2SO_4 solution, the obtained $^{15}NH_4^+$ was determined by ^1H nuclear magnetic resonance (^1H NMR, Bruker 600MHz). In detail, the pH of the electrolyte was firstly adjusted to 2, and then 425 μL of electrolyte was mixed with 50 μL DMSO-d6 and 25 μL maleic acid (10 ppm) as an internal standard for ^1H NMR measurement.

Determination of hydrazine: The content of hydrazine in the electrolyte was measured by the Watt and Chrisp method. The hydrazine (N_2H_4) color reagent was prepared by dissolving 5.99 g p-Dimethylaminobenzaldehyde in the mixture of 30 mL concentrated HCl and 300 mL ethanol. 3 mL above prepared color reagent was added into 3 mL electrolyte and then was stirred 10 min at room temperature in darkness. The absorbance of hydrazine in the resulting electrolyte was estimated at 460 nm. Absolute calibration was achieved using hydrazine

hydrate solutions of known concentration as standards, and the fitting curve shows a good linear relation of absorbance with $N_2H_4 \cdot$ concentration ($y = 0.018 + 1.151x$, $R^2=0.999$).

Determination of NO_3^-: In a typical procedure, 5.0 mL of standard or sample solutions were mixed with 0.10 mL of 1.0 M HCl. After shaking up and standing for 5 min, the concentration of NO_3^- was measured using a UV-vis spectrophotometer at a wavelength range from 200 nm to 300 nm. The absorbance of NO_3^- in the resulting electrolyte was estimated at 220 nm. Absolute calibration was achieved using $NaNO_3$ solutions of known concentration as standards, and the fitting curve shows a good linear relation of absorbance with NO_3^- $\cdot$ concentration ($y = 0.005 + 0.055x$, $R^2=0.999$).

Determination of NO_2^-: The NO_2^- color reagent A was prepared by dissolving 0.5 g sulfanilamide in 50.0 mL of 2.0 M HCl solution. The NO_2^- color reagent B was prepared by dissolving 20 mg N-(1-Naphthyl) ethylenediamine dihydrochloride in 20.0 mL of deionized water. Then 0.10 mL of color reagent A was added to 5.0 mL of standard or sample solutions. After mixing up and standing for 10 min, 0.10 mL of color reagent B was added to the above solution. The solution was then shaken up and standing for 30 min, and the concentration of NO_2^- was measured using a UV-vis spectrophotometer at wavelength range from 450 nm to 650 nm. The absorbance of NO_2^- in the resulting electrolyte was estimated at 540 nm. Absolute calibration was achieved using $NaNO_2$ solutions of known concentration as standards, and the fitting curve shows a good linear relation of absorbance with $NO_2^- \cdot$ concentration ($y = -0.003 + 1.133x$, $R^2=0.999$).

Calculation of NH₃ yield rate and Faradaic efficiency:

The NH$_3$ yield rate (R) was determined using the following equation:

$$R = \frac{C \cdot V}{t \cdot S}$$

(1)

where C is the measured NH$_3$ concentration, V is the volume of the electrolyte, t is the reaction time, and S is the catalyst loading mass.

The Faradaic efficiency (η) was determined using the following equation:

$$\eta = \frac{n \cdot F \cdot C \cdot V}{M \cdot Q}$$

(2)

where n is the number of electrons required for producing one NH$_3$ molecule ($n=3$), F is the Faraday constant ($F= 96485.33$), C is the measured NH$_3$ concentration, V is the volume of the electrolyte, M is the relative molecular mass of NH$_3$ ($M=17$), and the Q is the total charge passed through the electrodes.

The NH$_3$ partial current density (j) was determined using the following equation:

$$j = \frac{Q \cdot FE}{t \cdot m}$$

(3)

where Q is the total charge passed through the electrodes, FE is the Faradaic efficiency, t is the reaction time, and m is the geometrical area of the working electrode.

Supplementary Results
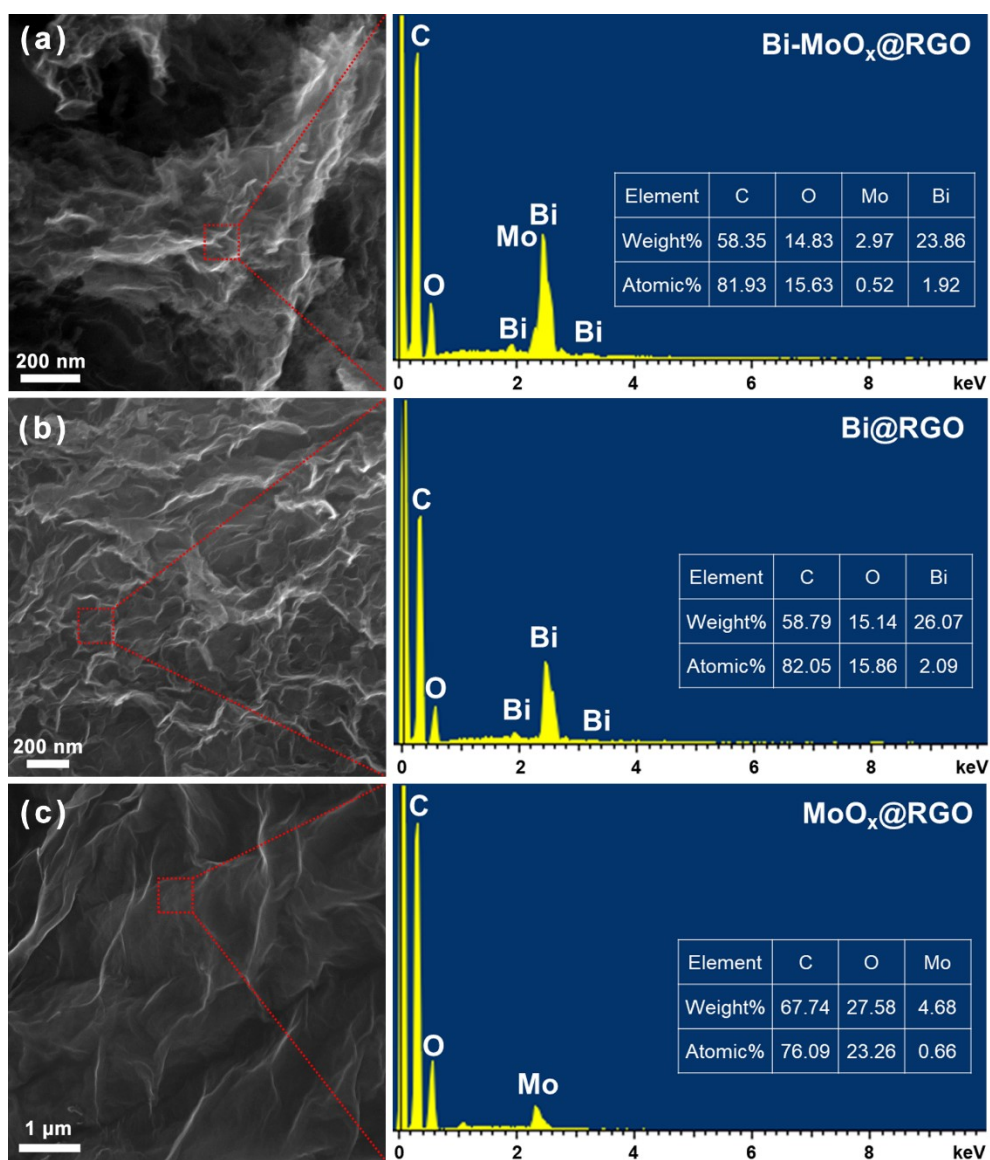
Fig. S1. SEM images and corresponding EDS analysis of (a) Bi-MoO$_x$@RGO, (b) Bi@RGO, and (c) MoO$_x$@RGO samples.
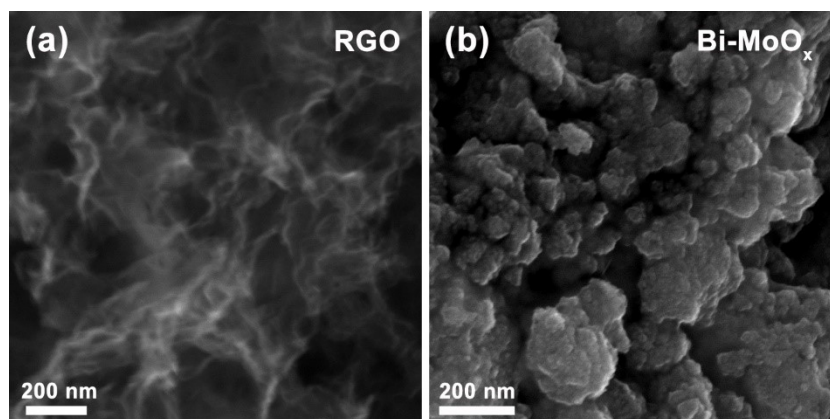
Fig. S2. SEM images of (a) RGO and (b) Bi-MoO$_x$ samples.
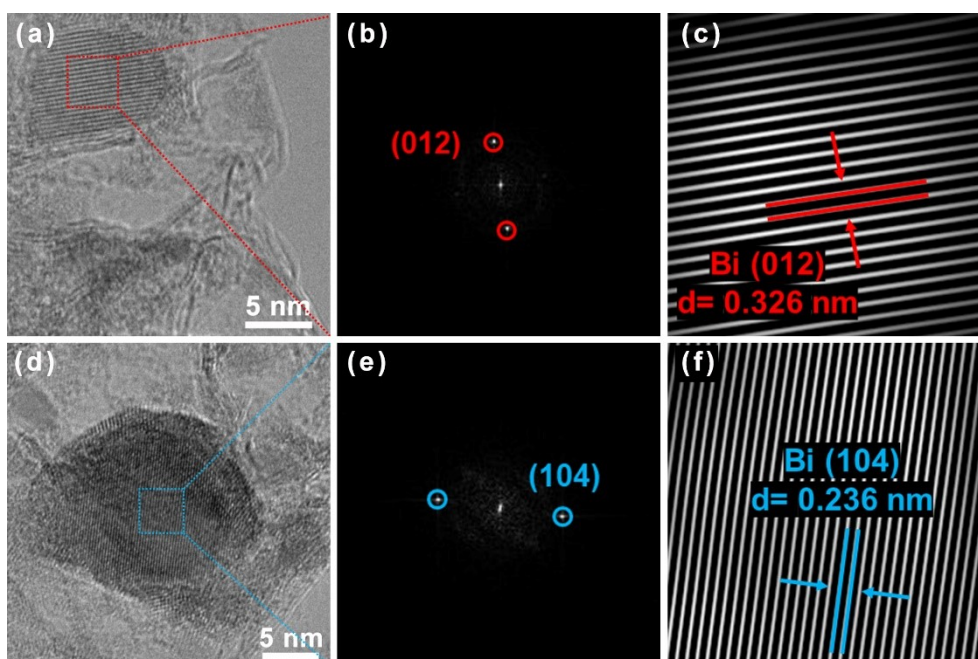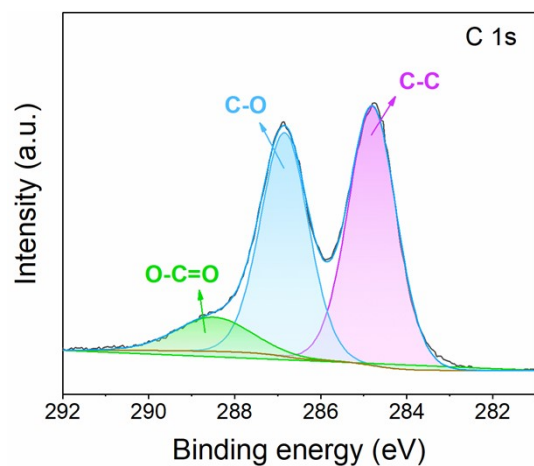

Fig. S3. (a, d) HRTEM images, (b, e) FFT patterns, and (c, f) corresponding IFFT patterns of

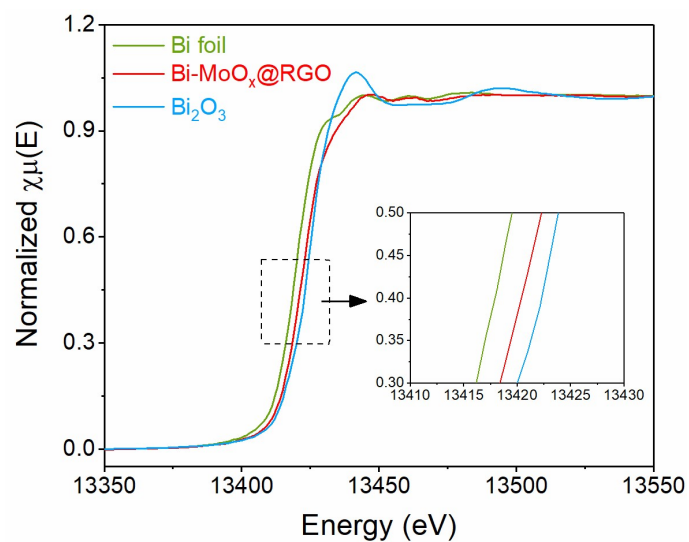the   Bi@RGO   sample.
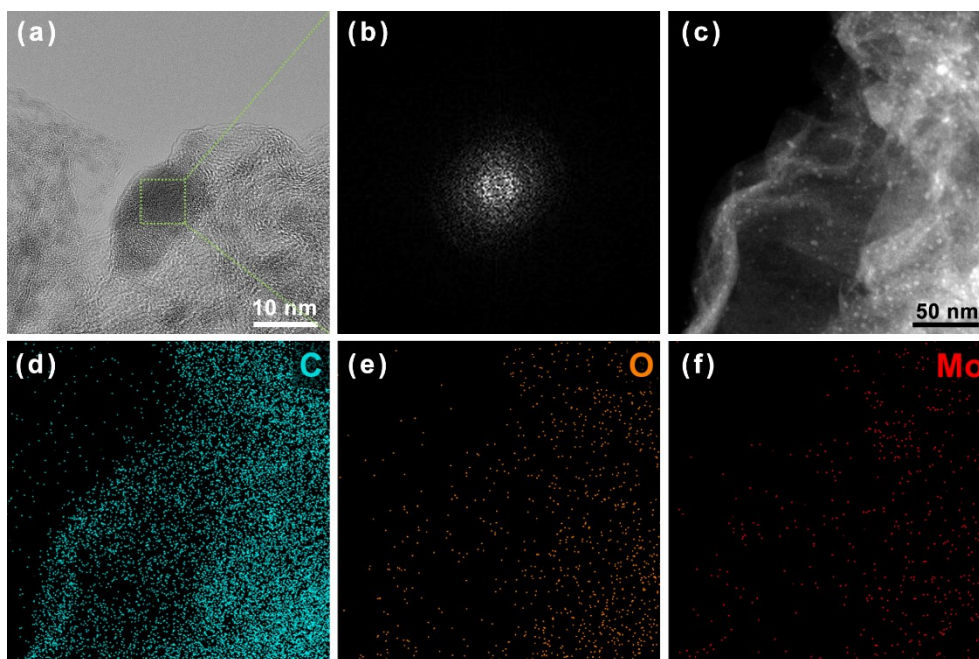
Fig. S4. (a) HRTEM image, (b) FFT pattern, (c) dark-field STEM image, and (d-f) corresponding elemental mapping images of MoO$_x$@RGO sample.
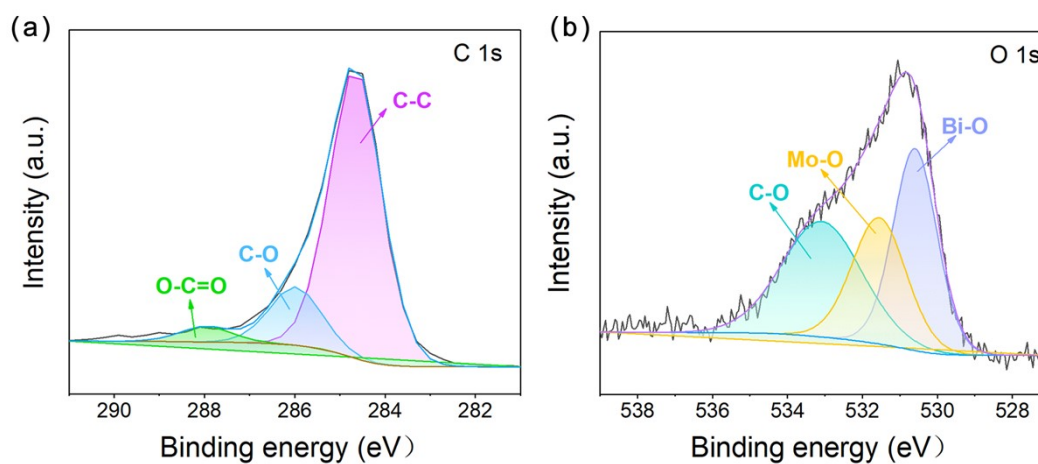
Fig. S5. X-ray photoelectron spectroscopy (XPS): (a) C 1s and (b) O 1s fine scan spectra of Bi-MoO$_x$@RGO sample.

Fig. S6. C 1s XPS fine scan spectra of GO sample.

Fig. S7. XANES spectra of Bi L_3-edge for the Bi foil, Bi-MoO$_x$@RGO, and Bi$_2$O$_3$.
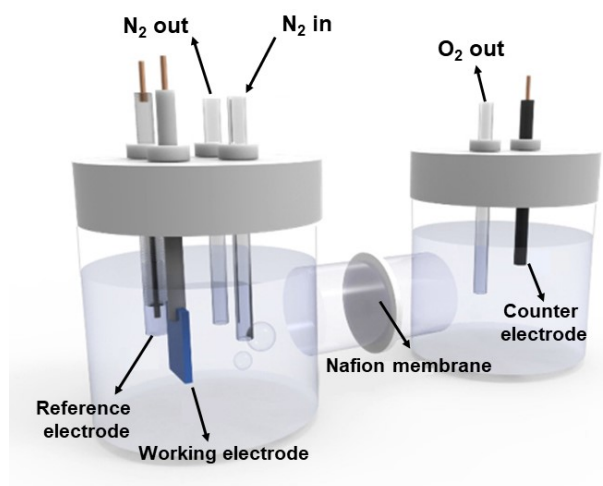
Fig. S8. Schematic illustration of the H-cell with a standard three-electrode system.
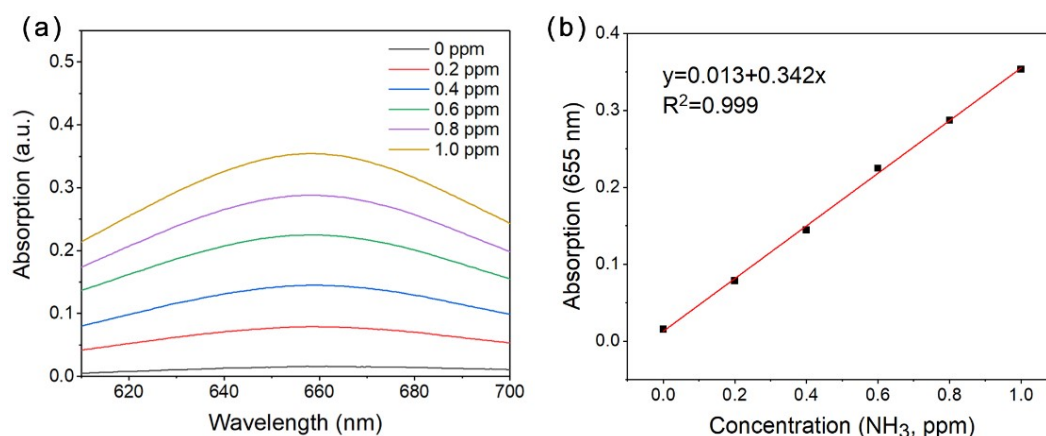
Fig. S9. Calibration curve of the indophenol blue method in 0.10 M Na_2SO_4 using NH_4Cl solutions with specific concentrations as standards. (a) UV-vis curves of indophenol assays with different concentrations of NH_3 after incubated for 2 hours and (b) calibration curve used for determining NH_3 concentration. The absorbance at 655 nm was measured by a UV-vis spectrophotometer, and the fitting curve shows a good linear correlation of absorbance with NH_3 concentration ($y = 0.013 + 0.342x$, $R^2=0.999$).
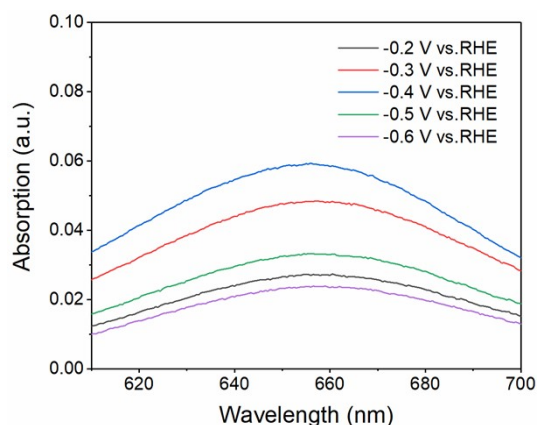
Fig. S10. UV-vis spectra of electrolytes in the cathodic chamber stained with the indophenol indicator after electrocatalytic NRR for 2 h on Bi-MoO$_x$@RGO catalysts at different potentials.
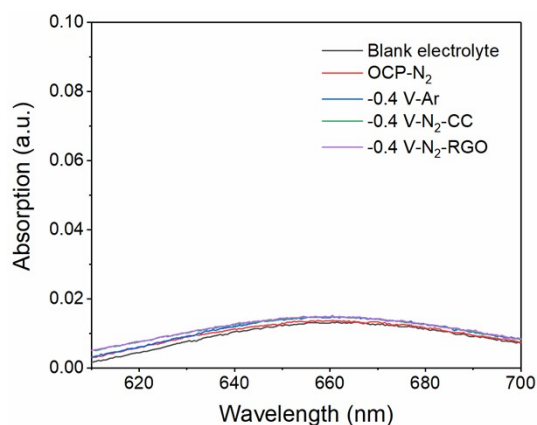

Fig. S11. UV-vis spectra of electrolytes stained with the indophenol indicator under different conditions. (Black line for blank electrolyte; red line for N$_2$ saturated electrolyte after electrolysis for 2 h on Bi-MoO$_x$@RGO catalysts at open-circuit potential (OCP); blue line for Ar saturated electrolyte after electrolysis for 2 h on Bi-MoO$_x$@RGO catalysts at -0.4 V vs. RHE; green line for N$_2$ saturated electrolyte after electrolysis 2 h on carbon cloth (CC) at -0.4 V vs. RHE.; purple line for N$_2$ saturated electrolyte after electrolysis for 2 h on RGO catalysts at -0.4 V vs. RHE)
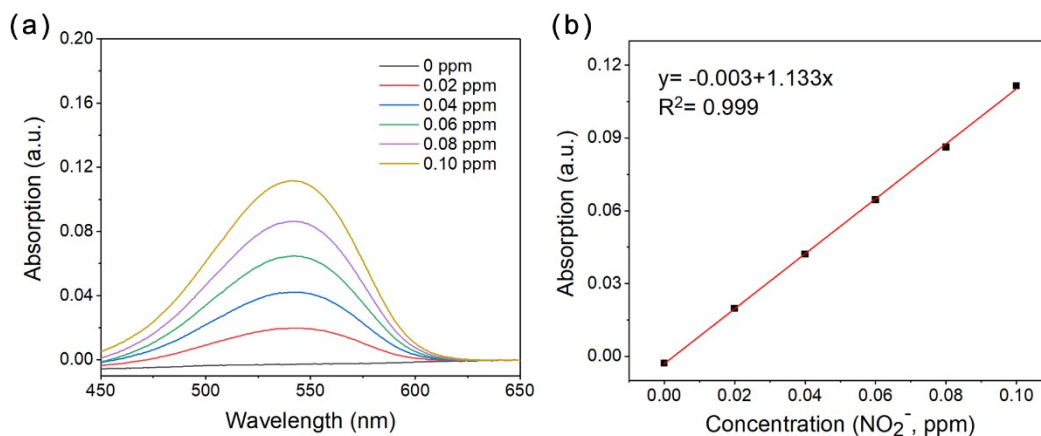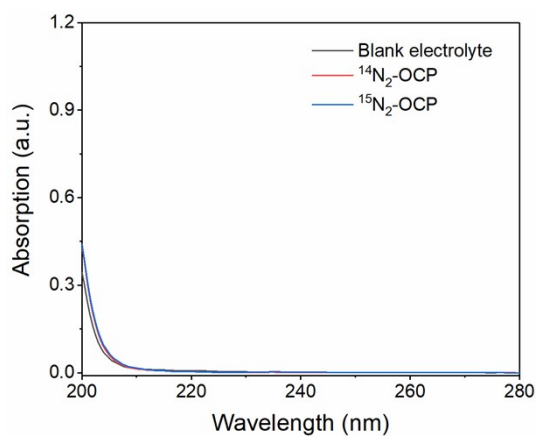
Fig. S12. Calibration for NO_2^- detection. (a) UV-vis curves of different concentrations of NO_2^- stained with the color indicator and (b) calibration curve used for estimation of NO_2^- concentration. The absorbance at 540 nm was measured by a UV-vis spectrophotometer, and the fitting curve shows a good linear correlation of absorbance with NO_2^- concentration ($y = -0.003 + 1.133x$, $R^2 = 0.999$).
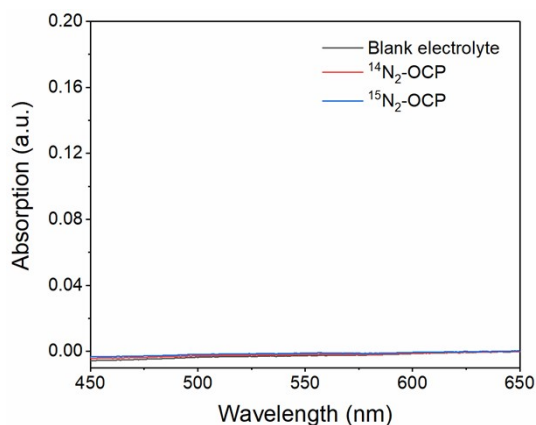
Fig. S13. UV-vis absorption spectra for determining the NO_2^- concentration in the blank electrolyte as well as electrolytes after being fed with $^{15}N_2$ or $^{14}N_2$ at open-circuit potential (OCP) for 2 h.
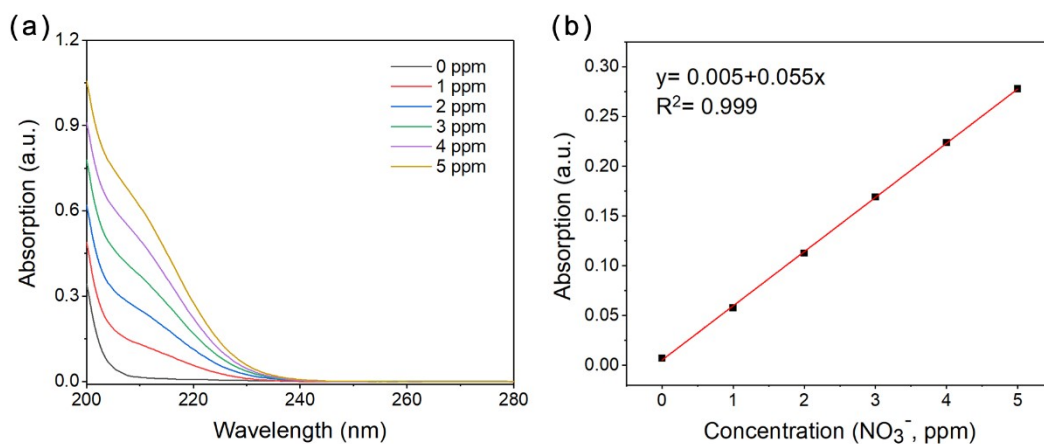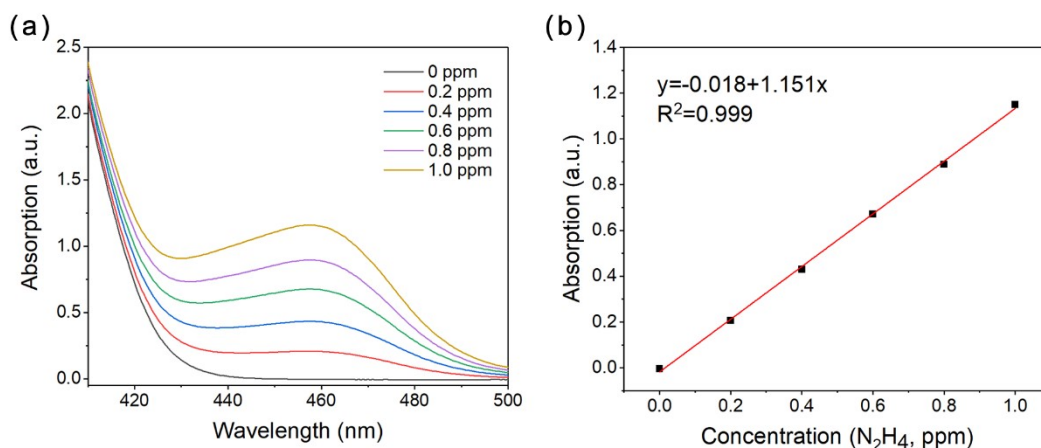
Fig. S14. Calibration for NO_3^- detection. (a) UV-vis curves of different concentrations of NO_3^- and (b) calibration curve used for estimation of NO_3^- concentration. The absorbance at 220 nm was measured by a UV-vis spectrophotometer, and the fitting curve shows a good linear correlation of absorbance with NO_3^- concentration ($y = 0.005 + 0.055x$, $R^2=0.999$).


Fig. S15. UV-vis absorption spectra for determining the NO_3^- concentration in the blank electrolyte as well as electrolytes after being fed with $^{15}N_2$ or $^{14}N_2$ at open-circuit potential (OCP) for 2 h.

16

Fig. S16. Calibration for N_2H_4 detection using the Watt and Chrisp method. (a) UV-vis curves of different concentrations of N_2H_4 stained with the color indicator and incubated for 10 min and (b) calibration curve used for estimation of N_2H_4 concentration. The absorbance at 460 nm was measured by a UV-vis spectrophotometer, and the fitting curve shows a good linear correlation of absorbance with N_2H_4 concentration ($y = 0.018 + 1.151x$, $R^2=0.999$).
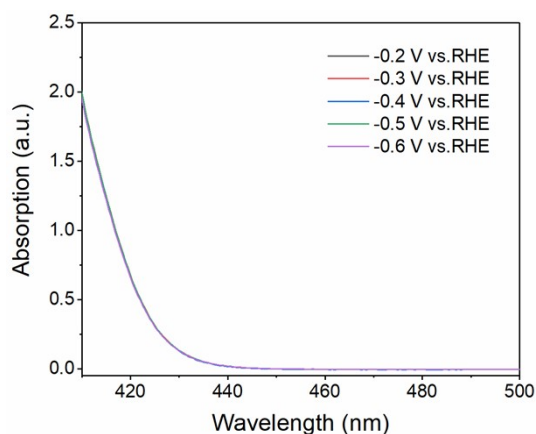

Fig. S17. UV-vis absorption spectra of the electrolytes stained with N_2H_4 color indicator after electrocatalytic NRR on Bi-MoO$_x$@RGO catalyst at different potentials.
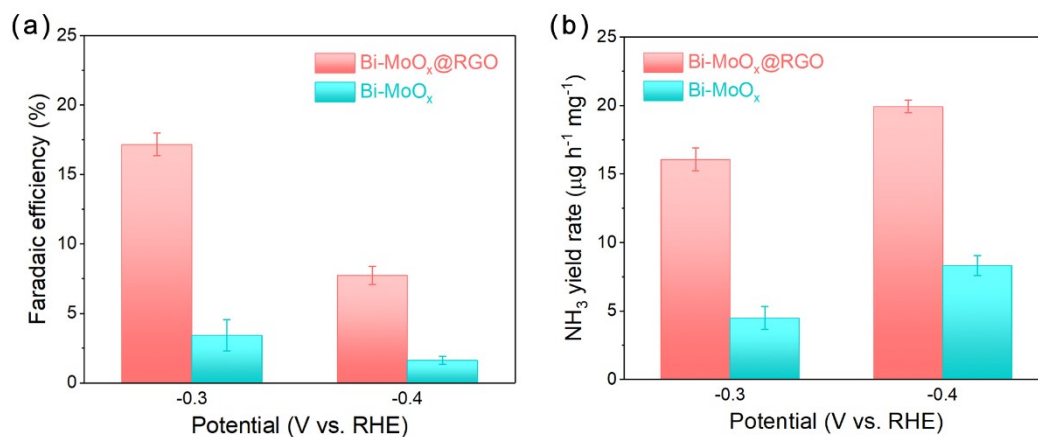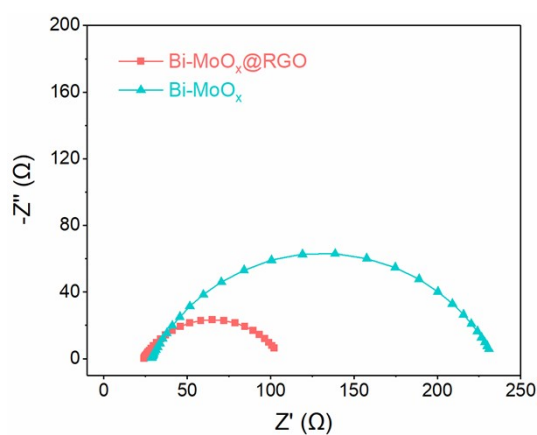
Fig. S18. (a) Faradaic efficiency, and (b) NH_3 yield rate of Bi-MoO$_x$@RGO and Bi-MoO$_x$ samples at different potentials.
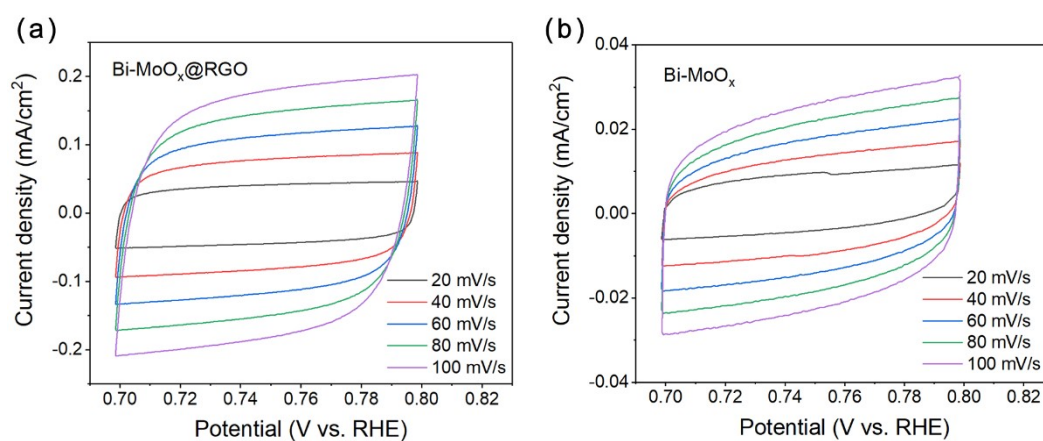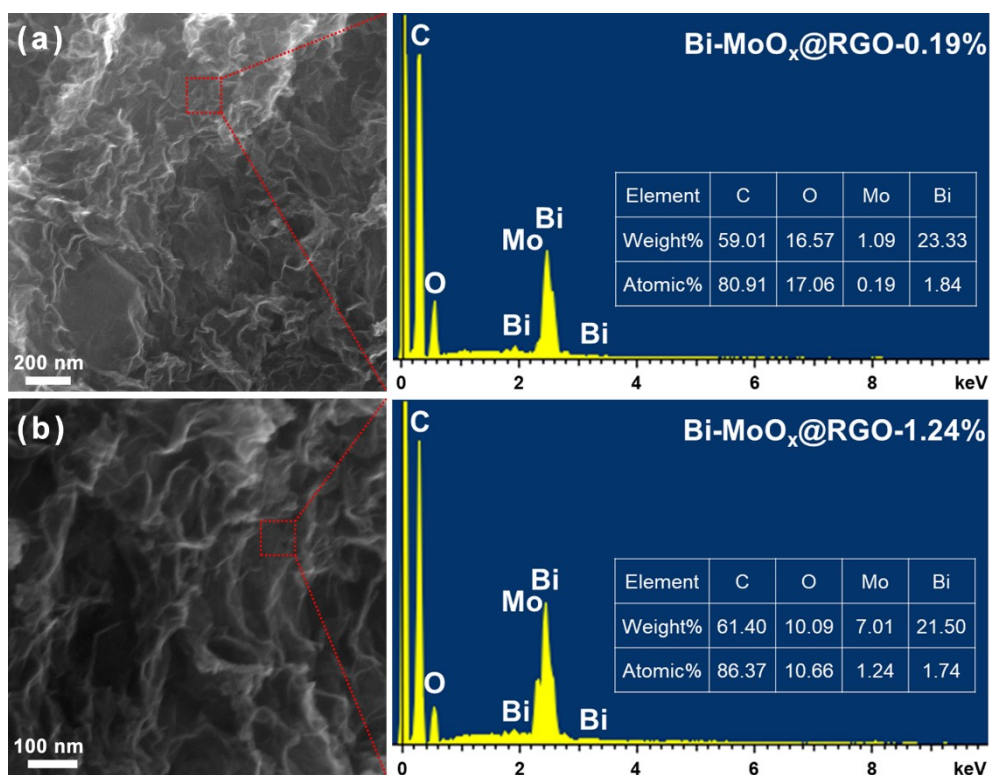

Fig. S19. Electrochemically active surface area (ECSA) analysis. Cyclic voltammetry (CV) curves of (a) Bi-MoO$_x$@RGO and (b) Bi-MoO$_x$ samples.
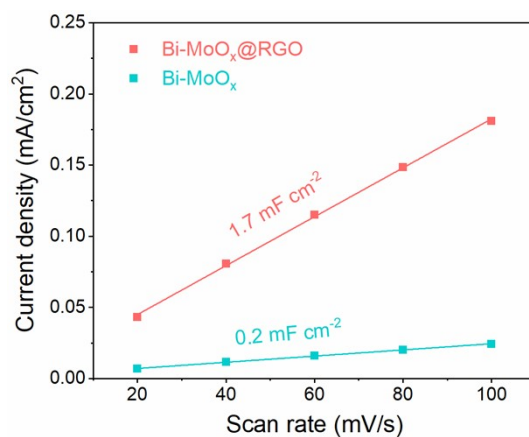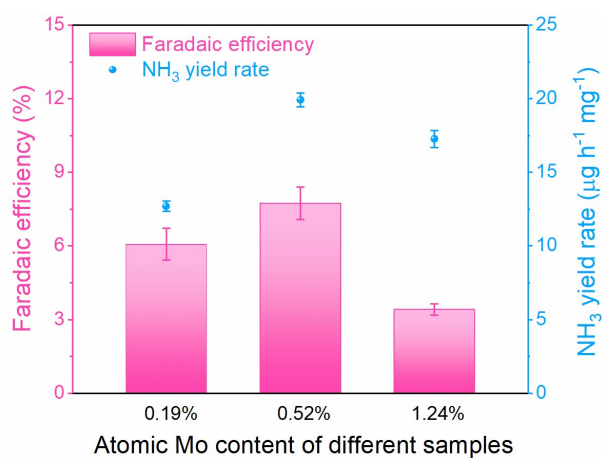
Fig. S20. Charging current density differences plotted against scan rates of cyclic voltammetry (CV) for Bi-MoO$_x$@RGO and Bi-MoO$_x$ samples.
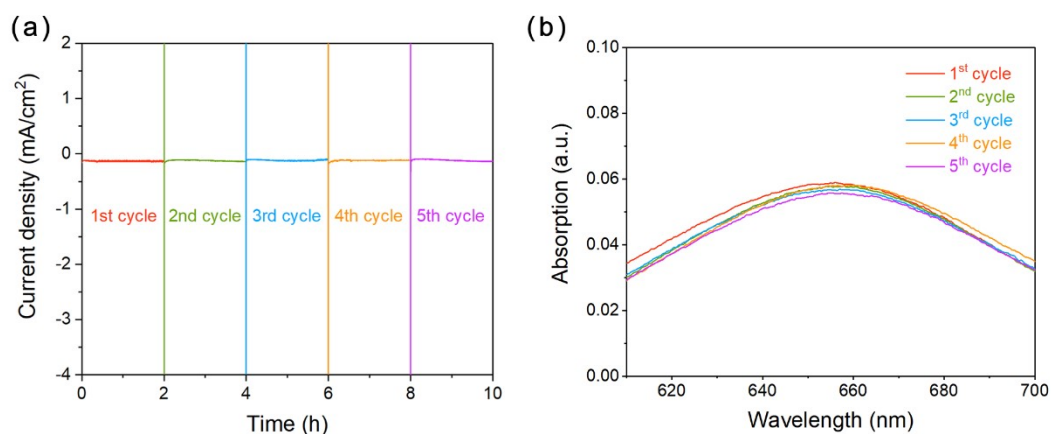

Fig. S21. Electrochemical impedance spectra (EIS) of Bi-MoO$_x$@RGO and Bi-MoO$_x$ samples.

Fig. S22. SEM images and corresponding EDS analysis of (a) Bi-MoO$_x$@RGO-0.19% and (b) Bi-MoO$_x$@RGO-1.24% samples.

Fig. S23. Faradaic efficiency and NH$_3$ yield rate of different samples with different atomic Mo content.

Fig. S24. (a) Chronoamperometry curves of the Bi-MoO$_x$@RGO catalyst at -0.4 V vs. RHE for five consecutive cycling tests. (b) UV-vis spectra of the electrolyte stained with indophenol indicator after each cycling test.
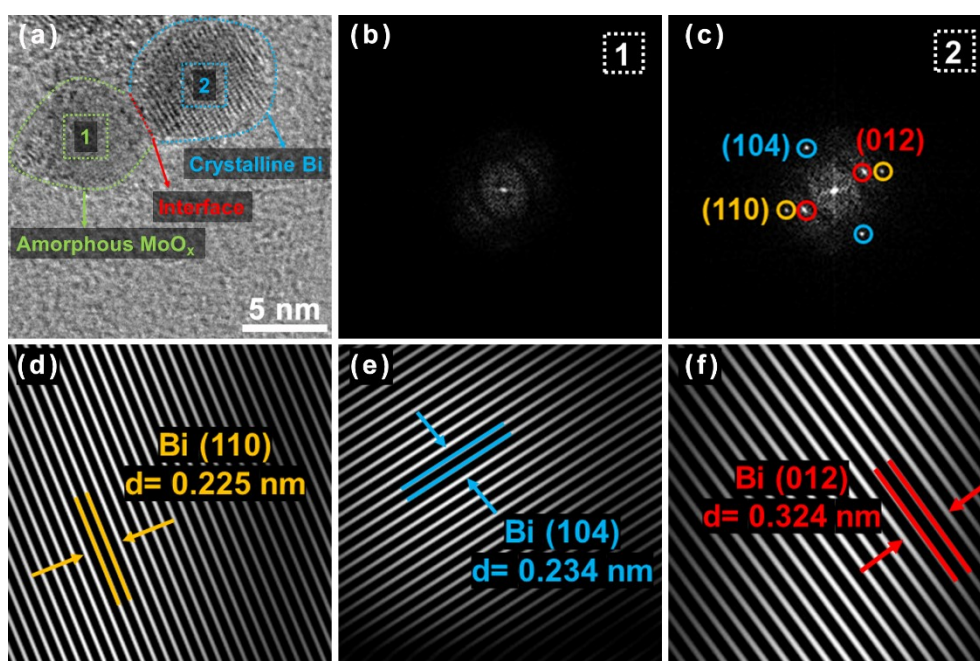
Fig. S25. (a) HRTEM image of the Bi-MoO$_x$@RGO catalyst after cycling tests. (b) FFT pattern measured at the region 1 in (a). (c) FFT pattern measured at the region 2 in (a). (d-f) Corresponding IFFT patterns of (c).
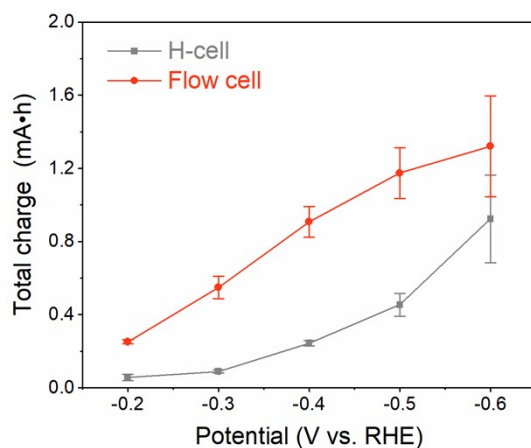
Fig. S26. Comparison of total charge passed through the electrode in the flow cell and the H-cell.
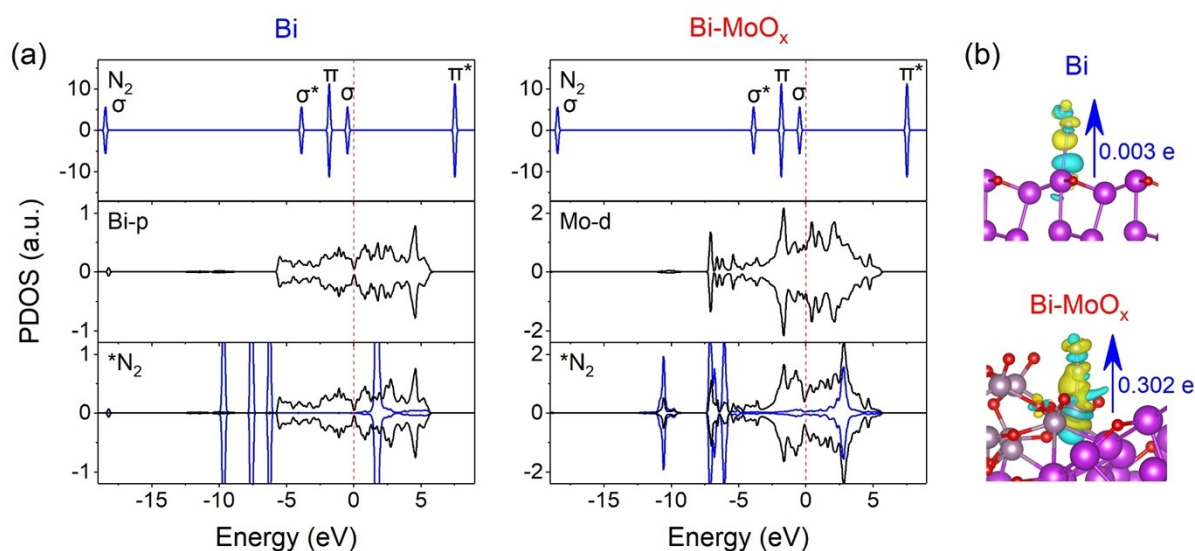
Fig. S27. (a) Projected density of states (PDOS) and (b) charge density differences of N_2 adsorbed on Bi and Bi-MoO$_x$ catalysts. The blue, cyan, red, and gray spheres represent Bi, Mo, O, and N atoms, respectively. The yellow and cyan regions represent electron accumulation and depletion, respectively. The isosurface values of N_2 adsorbed on Bi, and Bi-MoO$_x$ catalysts are 0.00002 and 0.0005 e/Å^3, respectively. The Fermi level is set to 0 eV.

Table S1. The relative atomic percentage of various functional groups in GO and Bi-MoO$_x$@RGO samples.

	O-C=O	C-O	C-C
GO	7.2%	43.8%	49.0%
Bi-MoO$_x$@RGO	4.2%	16.1%	79.7%

Table S2. Comparison of electrocatalytic NRR performance of the Bi-MoO$_x$@RGO catalyst with recently developed NRR electrocatalysts at ambient conditions.

Catalyst	NH$_3$ yield rate	Faradaic efficiency (%)	Data source
Bi-MoO$_x$@RGO	**19.93 μg h^{-1} mg^{-1}**	**17.17**	**This work**
1T''' MoS$_2$	9.09 μg h^{-1} mg^{-1}	13.60	[1] *Adv. Mater.* 2021
BiNi alloy	17.50 μg h^{-1} mg^{-1}	13.80	[2] *Angew. Chem. Int. Ed.* 2021
Bi@C	4.22 μg h^{-1} mg^{-1}	15.10	[3] *Adv. Funct. Mater.* 2021
MoO$_2$@C	9.75 μg h^{-1} mg^{-1}	3.24	[4] *Inorg. Chem.* 2021
Bi$_2$Te$_3$/C	3.90 μg h^{-1} cm^{-2}	7.90	[5] *Adv. Mater.* 2020
Bi nanoparticles	3.25 μg h^{-1} cm^{-2}	12.11	[6] *Adv. Energy Mater.* 2020
Bi nanosheets	12.49 μg h^{-1} mg^{-1}	7.09	[7] *ACS Sustainable Chem. Eng.* 2020
Bi-CeO$_2$	6.29 μg h^{-1} cm^{-2}	8.56	[8] *J. Phys. Chem. C* 2020
Bi$_5$O$_7$I nanotubes	3.15 μg h^{-1} cm^{-2}	13.42	[9] *Appl. Catal. B* 2020

Fe-MoS$_2$	8.63 μg h^{-1} mg^{-1}	18.8	[10] *Angew. Chem., Int. Ed.* 2020
Mo-Mo$_2$C/NCNTs	15.70 μg h^{-1} cm^{-2}	7.10	[11] *Adv. Mater.* 2020
MoP@rGO	7.50 μg h^{-1} mg^{-1}	9.1	[12] *Dalton Trans.* 2020
Defect-rich Bi	5.45 μg h^{-1} mg^{-1}	11.68	[13] *Angew. Chem. Int. Ed.* 2019
2D Bi nanosheet	2.54 μg h^{-1} cm^{-2}	10.46	[14] *ACS Catal.* 2019
Co-MoS$_{2-x}$	10.71 μg h^{-1} mg^{-1}	10.00	[15] *J. Am. Chem. Soc.* 2019
Fe-MoS$_2$/CC	12.50 μg h^{-1} cm^{-2}	10.80	[16] *J. Mater. Chem. A* 2019
MoO$_2$-OVs	12.20 μg h^{-1} mg^{-1}	8.20	[17] *Nano Energy* 2019
BiVO$_4$	8.60 μg h^{-1} mg^{-1}	10.04	[18] *Small Methods* 2018
Mo$_2$C/C	11.30 μg h^{-1} mg^{-1}	7.80	[19] *Adv. Mater.* 2018
MoS$_2$/CC	4.94 μg h^{-1} cm^{-2}	1.17	[20] *Adv. Mater.* 2018
Fe/Fe$_3$O$_4$	0.19 μg h^{-1} cm^{-2}	8.29	[21] *ACS Catal.* 2018
Ti$_3$C$_2$T$_x$ MXene	0.26 μg h^{-1} cm^{-2}	5.78	[22] *Joule* 2019

References

1   G. Lin, Q. Ju, X. Guo, W. Zhao, S. Adimi, J. Ye, Q. Bi, J. Wang, M. Yang and F. Huang, *Adv. Mater.*, 2021, **33**, e2007509.

2   Z. Fang, P. Wu, Y. Qian and G. Yu, *Angew. Chem. Int. Ed.*, 2021, **60**, 4275-4281.

3   Y. Wan, H. Zhou, M. Zheng, Z. H. Huang, F. Kang, J. Li and R. Lv, *Adv. Funct. Mater.*, 2021, **31**, 2100300.

4   Y. Du, Z. He, F. Ma, Y. Jiang, J. Wan, G. Wu and Y. Liu, *Inorg. Chem.*, 2021, **60**, 4116-4123.

5   N. Zhang, F. Zheng, B. Huang, Y. Ji, Q. Shao, Y. Li, X. Xiao and X. Huang, *Adv. Mater.*, 2020, **32**, e1906477.

6   D. Yao, C. Tang, L. Li, B. Xia, A. Vasileff, H. Jin, Y. Zhang and S. Z. Qiao, *Adv. Energy Mater.*, 2020, **10**, 2001289.

7   L. Xia, W. Fu, P. Zhuang, Y. Cao, M. O. L. Chee, P. Dong, M. Ye and J. Shen, *ACS Sustainable Chem. Eng.*, 2020, **8**, 2735-2741.

8   Y. Liu, C. Li, L. Guan, K. Li and Y. Lin, *J. Phys. Chem. C*, 2020, **124**, 18003-18009.

9   Y. Liu, B. Huang, X. Chen, Z. Tian, X. Zhang, P. Tsiakaras and P. K. Shen, *Appl. Catal., B*, 2020, **271**, 118919.

10   H. Su, L. Chen, Y. Chen, R. Si, Y. Wu, X. Wu, Z. Geng, W. Zhang and J. Zeng, *Angew. Chem. Int. Ed.*, 2020, **59**, 20411-20416.

11   Y. Ma, T. Yang, H. Zou, W. Zang, Z. Kou, L. Mao, Y. Feng, L. Shen, S. J. Pennycook, L. Duan, X. Li and J. Wang, *Adv. Mater.*, 2020, **32**, e2002177.

12   Y. Zhou, X. Yu, F. Sun and J. Zhang, *Dalton Trans.*, 2020, **49**, 988-992.

13   Y. Wang, M. M. Shi, D. Bao, F. L. Meng, Q. Zhang, Y. T. Zhou, K. H. Liu, Y. Zhang, J. Z. Wang, Z. W. Chen, D. P. Liu, Z. Jiang, M. Luo, L. Gu, Q. H. Zhang, X. Z. Cao, Y. Yao, M. H. Shao, Y. Zhang, X. B. Zhang, J. G. Chen, J. M. Yan and Q. Jiang, *Angew. Chem. Int. Ed.*, 2019, **58**, 9464-9469.

14   L. Li, C. Tang, B. Xia, H. Jin, Y. Zheng and S.-Z. Qiao, *ACS Catal.*, 2019, **9**, 2902-2908.

15   J. Zhang, X. Tian, M. Liu, H. Guo, J. Zhou, Q. Fang, Z. Liu, Q. Wu and J. Lou, *J. Am. Chem. Soc.*, 2019, **141**, 19269-19275.

16   X. Zhao, X. Zhang, Z. Xue, W. Chen, Z. Zhou and T. Mu, *J. Mater. Chem. A*, 2019, **7**, 27417-27422.

17   G. Zhang, Q. Ji, K. Zhang, Y. Chen, Z. Li, H. Liu, J. Li and J. Qu, *Nano Energy*, 2019, **59**, 10-16.

18   J. X. Yao, D. Bao, Q. Zhang, M. M. Shi, Y. Wang, R. Gao, J. M. Yan and Q. Jiang, *Small Methods*, 2018, **3**.

19   H. Cheng, L. X. Ding, G. F. Chen, L. Zhang, J. Xue and H. Wang, *Adv. Mater.*, 2018, **30**, e1803694.

20   L. Zhang, X. Ji, X. Ren, Y. Ma, X. Shi, Z. Tian, A. M. Asiri, L. Chen, B. Tang and X. Sun, *Adv. Mater.*, 2018, **30**, e1800191.

21   L. Hu, A. Khaniya, J. Wang, G. Chen, W. E. Kaden and X. Feng, *ACS Catal.*, 2018, **8**, 9312-9319.

22   Y. Luo, G.-F. Chen, L. Ding, X. Chen, L.-X. Ding and H. Wang, *Joule*, 2019, **3**, 279-289.